

Is shrub expansion into grasslands pushed or pulled? A  
spatial integral projection model for woody plant  
encroachment

Trevor Drees<sup>\*a,b</sup>, Brad M. Ochocki<sup>b</sup>, Scott L. Collins<sup>c</sup>, and Tom E.X. Miller<sup>b</sup>

<sup>a</sup>Department of Biology, Penn State University, State College, PA USA

<sup>b</sup>Program in Ecology and Evolutionary Biology, Department of BioSciences, Rice  
University, Houston, TX USA

<sup>c</sup>Department of Biology, University of New Mexico, Albuquerque, NM USA

July 12, 2022

---

<sup>\*</sup>thd5066@psu.edu

# 1 Abstract

2 **Encroachment**<sup>1</sup> of shrubs into adjacent grasslands has become an increasingly reported  
3 phenomenon across the world, and such encroachment is either pulled forward by high  
4 population growth at the low-density encroachment front or pushed forward by higher-  
5 density areas behind the front. However, at sites such as Sevilleta National Wildlife  
6 Refuge in central New Mexico, little is known about whether encroachment is pushed or  
7 pulled, and the dynamics of encroachment are not well-understood. Here, long-term en-  
8 croachment of creosotebush (*Larrea tridentata*), a native perennial shrub, stands in stark  
9 contrast with the stagnation in encroachment observed in recent decades. In order to  
10 better understand creosotebush encroachment at this site, we quantify it using a spatially  
11 structured population model where a wave of individuals travels at a speed governed by  
12 both dispersal and density-dependence. Results indicate that population growth rates  
13 generally increase with decreasing density, suggesting that encroachment is pulled by  
14 individuals at the low-density wave front, and the spatial population model predicts an  
15 encroachment rate of less than 2 cm per year. While the predicted rate of encroach-  
16 ment is consistent with observations over recent decades, it does not explain long-term  
17 creosotebush encroachment at the study site, suggesting that this process may occur in  
18 pulses when recruitment, seedling survival, or dispersal significantly exceed typical rates.  
19 Overall, our work demonstrates that individuals at low densities are likely the biggest  
20 contributors to creosotebush encroachment at this site, and that this encroachment is  
21 likely a process that occurs in large but infrequent bursts rather than at a steady pace.

## 22 Keywords

23 density-dependence, ecotones, woody encroachment, shrubs, integral projection model,  
24 grassland

---

<sup>1</sup>*I am not editing the abstract for now.*

## 25 Introduction

26 The recent and ongoing encroachment of shrubs and other woody plants into adjacent  
27 grasslands has caused significant vegetation changes across arid and semi-arid landscapes  
28 worldwide (Van Auken, 2000, 2009; Goslee et al., 2003; Gibbens et al., 2005; Parizek et al.,  
29 2002; Cabral et al., 2003; Trollope et al., 1989; Roques et al., 2001). The process of en-  
30 croachment generally involves increases in the number or density of woody plants in both  
31 time and space (Van Auken, 2000), which can drive shifts in plant community structure  
32 and alter ecosystem processes (Schlesinger et al., 1990; Ravi et al., 2009; Schlesinger  
33 and Pilmanis, 1998; Knapp et al., 2008). Other effects of encroachment include changes  
34 in ecosystem services (Reed et al., 2015; Kelleway et al., 2017), declines in biodiversity  
35 (Ratajczak et al., 2012; Sirami and Monadjem, 2012; Brandt et al., 2013), and economic  
36 losses in areas where the proliferation of shrubs adversely affects grazing land and pastoral  
37 production (Mugasi et al., 2000; Oba et al., 2000).

38 Woody plant encroachment can be studied through the lens of spatial population  
39 biology as a wave of individuals that may expand across space and over time (Kot et al.,  
40 1996; Neubert and Caswell, 2000; Wang et al., 2002; Pan and Lin, 2012). Theory pre-  
41 dicts that the speed of wave expansion depends on two processes: local demography and  
42 dispersal of propagules. First, local demographic processes include recruitment, survival,  
43 growth, and reproduction, which collectively determine the rate at which newly colonized  
44 locations increase in density and produce new propagules. Second, colonization events  
45 are driven by the spatial dispersal of propagules, which is commonly summarized as a  
46 probability distribution of dispersal distance, or “dispersal kernel”. The speed at which  
47 expansion waves move is highly dependent upon the shape of the dispersal kernel, espe-  
48 cially long-distance dispersal events in the tail of the distribution (Skarpaas and Shea,  
49 2007). Both demography and dispersal may depend on plant size, since larger plants  
50 often have improved demographic performance and release seeds from greater heights,

51 leading to longer dispersal distances (Nathan et al., 2011). Accounting for population  
52 structure, including size structure, may therefore be important for understanding and  
53 predicting wave expansion dynamics (Neubert and Caswell, 2000).

54 Theory predicts that the nature of conspecific density dependence is another critical  
55 feature of expansion dynamics but this is rarely studied in the context of woody plant  
56 encroachment. Expansion waves typically correspond to gradients of conspecific density  
57 – high in the back and low at the front – and demographic rates may be sensitive to  
58 density due to intraspecific interactions like competition or facilitation. If the demo-  
59 graphic effects of density are strictly negative due to competitive effects that increase  
60 with density then demographic performance is maximized as density goes to zero, at the  
61 leading edge of the wave. Under these conditions, the wave is “pulled” forward by indi-  
62 viduals at the low-density vanguard (Kot et al., 1996), and targeting these individuals  
63 and locations would be the most effective way to slow down or prevent encroachment  
64 (cite?). However, woody encroachment systems often involve positive feedbacks whereby  
65 shrub establishment modifies the environment in ways that facilitate further shrub re-  
66 cruitment. For example, woody plants can modify their micro-climates in ways that  
67 elevate nighttime minimum temperatures, promoting conspecific recruitment and sur-  
68 vival for freeze-sensitive species (D’Odorico et al., 2010; Huang et al., 2020). Positive  
69 density dependence (or Allee effects) causes demographic rates to be maximized at higher  
70 densities behind the leading edge, which “push” the expansion forward, leading to qualita-  
71 tively different expansion dynamics (Kot et al., 1996; Taylor and Hastings, 2005; Sullivan  
72 et al., 2017; Lewis and Kareiva, 1993; Veit and Lewis, 1996; Keitt et al., 2001). Pushed  
73 expansion waves generally have different shapes (steeper density gradients) and slower  
74 speeds than pulled waves (Gandhi et al., 2016), and may require different strategies for  
75 managing or decelerating expansion (check Taylor and Hastings ref). The potential for  
76 positive feedbacks is well documented in woody encroachment systems but it remains un-  
77 clear whether and how strongly these feedbacks decelerate shrub expansion and influence

78 strategies for management of woody encroachment.

79     In this study, we linked woody plant encroachment to ecological theory for invasion  
80 waves, with the goals of understanding how seed dispersal and density-dependent demog-  
81 raphy drive encroachment, and determining whether the encroachment wave is pushed or  
82 pulled. Throughout the aridlands of the southwestern United States, shrub encroachment  
83 into grasslands is well documented (D’Odorico et al., 2012) but little is known about the  
84 dispersal and demographic processes that govern it. Our work focused on encroachment  
85 of creosotebush (*Larrea tridentata*) in the northern Chihuahuan Desert. Expansion of  
86 this species into grasslands over the past 150 years has been well documented, leading to  
87 decreased cover of *Bouteloua eriopoda*, the dominant foundation species of Chihuahuan  
88 desert grassland (Gardner, 1951; Buffington and Herbel, 1965; Gibbens et al., 2005).  
89 As in many woody encroachment systems, creosotebush expansion generates ecotones  
90 marking a transition from dense shrubland to open grassland, with a transition zone in  
91 between where shrubs can often be found interspersed among grasses (Fig. 1).

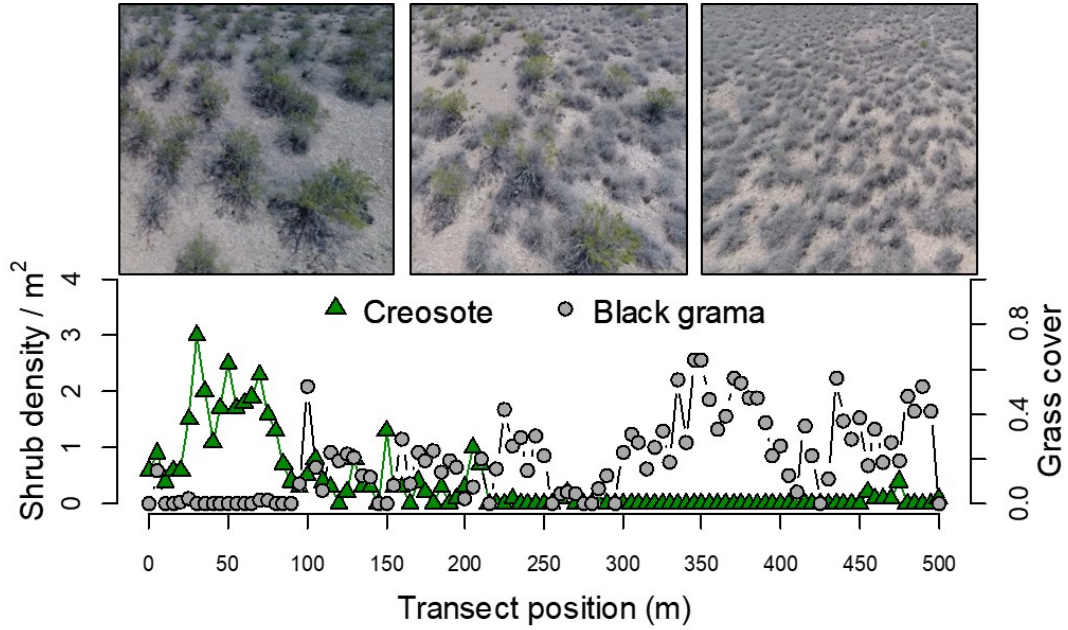


Figure 1: Example of an ecotone transect at Sevilleta LTER, spanning gradients of creosotebush and black grama grass. Photo credits: TEX Miller

Historically, creosotebush encroachment into grasslands is believed to have been driven by a combination of factors including overgrazing, drought, variability in rainfall, and suppression of fire regimes Moreno-de las Heras et al. (2016). These shrubs are also thought to further facilitate their own encroachment through positive feedbacks (Grover and Musick, 1990; D’Odorico et al., 2012) by modifying their environment in ways that favor continued growth and recruitment, including changes to the local micro-climate (D’Odorico et al., 2010) and rates of soil erosion (Turnbull et al., 2010). Such positive feedback also involve suppression of herbaceous competitors, reducing competition as well as the amount of flammable biomass used to fuel the fires that keep creosotebush growth in check (Van Auken, 2000). We hypothesized that, given potential for positive feedback mechanisms, the rarity of conspecifics at the low-density encroachment front may depress demographic performance and generate pushed-wave dynamics.

104 We used a combination of observational and experimental data from shrub ecotones  
 105 in central New Mexico to parameterize a spatial integral projection model (SIPM) that  
 106 predicts that speed of encroachment ( $m/yr$ ) resulting from lower-level demographic and  
 107 dispersal processes. Our data came from demographic surveys and experimental trans-  
 108 plants along replicate ecotone transects spanning a gradient of shrub density, and seed  
 109 drop experiments to estimate the properties of the dispersal kernel. We focused on wind  
 110 dispersal of seeds, since little is known about the natural history of dispersal in this  
 111 system and the seeds lack rewards to attract animal dispersers. We also used re-surveys  
 112 of permanents transects as an independent measure of encroachment that provided a  
 113 benchmark against which to evaluate model predictions. The SIPM accounts for size-  
 114 structured demography of creosotebush, allows us to test whether shrub expansion is  
 115 pulled by the low-density front or pushed from the high-density core, and identifies the  
 116 local (demographic) and spatial (seed dispersal) life cycle transitions that most strongly  
 117 contribute to expansion speed<sup>2</sup>. We address the following specific questions:

- 118 1. What is the nature of conspecific density dependence in demographic vital rates  
 119 along shrub encroachment ecotones? Is encroachment pulled by the individuals at  
 120 the front or pushed by individuals behind it?
- 121 2. What is the seed dispersal kernel for this species and how does this vary with  
 122 maternal plant size?
- 123 3. What is the predicted rate of expansion from the SIPM and which lower-level  
 124 processes most strongly affect the expansion speed?
- 125 4. How does the observed rate of encroachment in the recent past compare to model  
 126 predictions?

---

<sup>2</sup>*we will need to stay consistent with the language of encroachment/expansion/invasion. For now I am swictihg a lot.*

## 127 **Materials and methods**

### 128 **Study species**

129 Creosotebush *Larrea tridentata* is a perennial, drought-resistant shrub that is native to  
130 the arid and semiarid regions of the southwestern United States and northern Mexico.  
131 High-density areas of creosotebush consist largely of barren soil between plants due to  
132 the “islands of fertility” these shrubs create around themselves (Schlesinger et al., 1996;  
133 Reynolds et al., 1999), though lower-density areas will often contain grasses in the inter-  
134 shrub spaces (Fig. 1). In our northern Chihuahuan desert study region creosotebush  
135 reproduces sexually, with numerous small yellow flowers giving rise to highly pubescent  
136 spherical fruits several millimetres in diameter; these fruits consist of five carpels, each  
137 of which contains a single seed. Seeds are dispersed from the parent plant by gravity and  
138 wind, with the possibility for seeds to subsequently be transported by animals or water  
139 (Maddox and Carlquist, 1985). In other regions, this species also reproduces asexually  
140 and can give rise to long-lived clonal stands (Vasek, 1980), but this does not occur in our  
141 study region. The foliage is dark green, resinous, and unpalatable to most grazing and  
142 browsing animals (Mabry et al., 1978).

### 143 **Study site**

144 We conducted our work at the Sevilleta National Wildlife Refuge (SNWR), a Long-Term  
145 Ecological Research (SEV-LTER) site in central New Mexico. The refuge exists at the in-  
146 tersection of several eco-regions, including the northern Chihuahuan Desert, Great Plains  
147 grassland, and steppes of the Colorado Plateau. Annual precipitation is approximately  
148 250 mm, with the majority falling during the summer monsoon season from June to  
149 September. The recruitment events that facilitate creosotebush expansion are thought  
150 to be highly episodic (Peters and Yao, 2012), and this may be linked to fluctuations in  
151 monsoon precipitation (Boyd and Brum, 1983; Bowers et al., 2004). Monsoon precipita-



tion during the study years (2013-2017) was [summarise climate data].

## Demographic data

### Ecotone transects

We collected demographic data during early June of every year from 2013-2017. This work was conducted at **four sites in the eastern part of SNWR**<sup>3</sup> (one site was initiated in 2013 and the other three in 2014), with three transects at each site. All transects were situated along a shrubland-grassland ecotone so that a full range of shrub densities was captured: each transect spanned core shrub areas, grassland with no or few shrubs, and the transition between them. Lengths of these transects varied from 200 to 600 m, determined by the strength of vegetation transition since “steep” transitions required less length to capture the full range of shrub density.

We quantified shrub density in 5-meter “windows” along each transect, including all shrubs within one meter of the transect on either side (shrubs that partially overlapped with the census area were included). Densities were quantified once for each transect (in 2013 or 2014) and were assumed to remain constant for the duration of the study, a reasonable assumption for a species with very low recruitment and very high survival of established plants. Given the population’s size structure, we weighted the density of each window by the sizes of the plants, which we quantified as volume (cm<sup>3</sup>). Volume was calculated as that of an elliptic cone:  $V_i = \frac{\pi h}{3} \frac{lw}{4}$  where  $l$ ,  $w$ , and  $h$  are the maximum length, maximum width, and height, respectively. Maximum length and width were measured so that they were always perpendicular to each other, and height was measured from the base of the woody stem at the soil surface to the tallest part of the shrub. The weighted density for a window was then expressed as log(volume) summed over all plants in the window.

---

<sup>3</sup>*would a map be helpful?*

## 176 **Observational census**

177 At approximately 50-m intervals along each transect we tagged up to 10 plants for an-  
178 nual demographic census and recorded their local (5-m resolution) window so that we  
179 could connect individual demographic performance to local density. These tagged shrubs  
180 were revisited every June and censused for survival (alive/dead), size (width, length, and  
181 height, as above), flowering status, and fertility of flowering plants (numbers of flower-  
182 buds, flowers, and fruits). In instances where shrubs had large numbers of reproductive  
183 structures that would be difficult to reliably count (a large shrub may have thousands  
184 of flowers or fruits), we made counts on a fraction of the shrub and extrapolated to es-  
185 timate whole-plant reproduction. Creosotebush does not have one discrete reproductive  
186 event per year; instead, flowering may occur throughout much of the warm season. By  
187 combining counts of buds, flowers, and fruits we intended to capture a majority of the  
188 season's reproductive output, assuming that all buds and flowers will eventually become  
189 fruits. Our measurements of reproductive output are therefore conservative and may un-  
190 derestimate total seed production for an entire transition year. Each year, we searched  
191 for new recruits within one  $m$  on either side of the transect. New recruits were tagged  
192 and added to the demographic census. The observational census included a total of 522  
193 unique individuals.

## 194 **Transplant experiment**

195 We conducted a transplant experiment in 2015 to test how shrub density affects seedling  
196 survival. This approach complemented observational estimates of density dependence  
197 and filled in gaps for a part of the shrub life cycle that was rarely observed due to low  
198 recruitment. Seeds for the experiment were collected from plants in our study popu-  
199 lation in 2014. Seeds were germinated on Pro-Mix potting soil (Quakertown, PA) in  
200 Fall 2014 and seedlings were transferred to 3.8 cm-by-12.7 cm cylindrical containers and  
201 maintained in a greenhouse at Rice University. Seedlings were transported to SNWR

202 and transplanted into the experiment during July 27-31, 2015. Transplant timing was  
203 intended to coincide with the monsoon season, when most natural recruitment occurs.

204 The transplant experiment was conducted at the same four sites and three transects  
205 per site as the observational demographic census, where we knew weight shrub densities  
206 at 5-m window resolution. We established 12 1-m by 1-m plots along each transect.  
207 Plots were intentionally placed to capture density variation: four plots were in windows  
208 with zero shrubs, four plots were placed in the top four highest-density windows on the  
209 transect, and the remaining four plots were randomly distributed among the remaining  
210 windows with weighted density greater than zero. Plots were placed in the middle of  
211 each 5-m window (at meter 2.5) and were divided into four 0.5-m by 0.5-m subplots. We  
212 divided each subplot into nine squares (0.125-m by 0.125-m) and recorded ground cover  
213 of each square as one of the following categories: bare ground, creosotebush, black grama  
214 (*B. eriopoda*), blue grama (*B. gracilis*), other grass, or “other”. Each subplot received one  
215 transplanted shrub seedling, for a total of 48 transplants per transect, 144 transplants  
216 per site, and 576 transplants in the entire experiment. Each site was set up on a different  
217 day and there was a significant monsoon event after the third and before the fourth  
218 site. This resulted in differential mortality that appears to be related to site (captured  
219 as a statistical random effect) but more likely reflects the timing of the monsoon event  
220 relative to planting (moist soil likely promoted transplant survival). We revisited the  
221 transplant experiment on October 24, 2015 to survey mortality. After that first visit,  
222 transplants were censused along with the naturally occurring plants each June, following  
223 the methods described above.

## 224 **Demographic analysis**

225 We fit statistical models to the demographic data and used AIC-based model selection to  
226 evaluate empirical support for alternative candidate models. The top statistical models  
227 were then used as the vital rate sub-models of the SIPM, so there is a strong connection

between the statistical and population modeling, as is typical of integral projection modeling. Our analyses focused on the following demographic vital rates: survival, growth, probability of flowering, fertility (flower and fruit production), seedling recruitment, and seedling size. Most of these vital rates were modeled as a function of plant size, and all of them included the possibility of density dependence.

The alternative hypotheses of pushed versus pulled wave expansion rest on how the rate of population increase ( $\lambda$ ), derived from the combination of all vital rates, respond to density. We were particularly interested in whether demographic performance was maximized as local density goes to zero (pulled) or at non-zero densities behind the wave front (pushed). To flexibly model density dependence and detect non-monotonic responses, we used generalized additive models in the R package ‘mgcv’ (Wood, 2017). For each vital rate, we fit candidate models with or without a smooth term for local weighted density (among other possible covariates). To avoid over-fitting, we set the ‘gamma’ argument of `gam()` to 1.8, which increases the complexity penalty, results in smoother fits (Wood, 2017), and makes our approach more conservative (other gamma values yielded qualitatively similar results). We pooled data across transition years for analysis. All models included the random effect of transect (12 transects across 4 sites); we did not attempt to model both site and transect-within-site random effects due to the low numbers of each. All vital rate functions used the natural logarithm of volume ( $\text{cm}^3$ ) as the size variable and the sum of  $\log(\text{volume})$  as the weighted density of a transect window.

**Survival** We modeled survival or mortality in year  $t+1$  as a Bernoulli random variable with three candidate models for survival probability. These included smooth terms for initial size in year  $t$  only (1), initial size and weighted density (2), and both smooth terms plus an interaction between initial size and weighted density (3). We analyzed survival of experimental transplants and observational census plants together in the same analyses,

with a fixed effect of transplant status (yes/no) included in all candidate models. Since recruits and thus mortality events were both very rare in the observational survey, this approach allowed us to “borrow strength” over both data sets to generate a predictive function for size- and possibly density-dependent survival while statistically accounting for differences between experimental and naturally occurring plants. Because we had additional, finer-grained cover data for the transplant experiment that we did not have for the observational census, we conducted an additional stand-alone analysis of transplant survival that explored the influence of covariates at multiple spatial scales (Appendix).

**Growth** We modeled size in year  $t + 1$  as a Gaussian random variable. There were nine candidate models for growth. The simplest model (1) defined the mean of size in year  $t + 1$  as a smooth function of size in year  $t$  and constant variance. Models (2) and (3) had constant variance but the mean included smooth terms for initial size and weighted density (2) or both smooth terms plus an interaction between initial size and weighted density (3). Models 4-6 had the same mean structure as 1-3 but defined the standard deviation of size in year  $t + 1$  as a smooth function of initial size. Models 7-9 mirrored 4-6 and additionally included a smooth term for weighted density in the standard deviation. Modeling growth correctly is important because it defines the probability of any future size conditional on current size, a critical element of the IPM transition kernel. We verified that the AIC-selected model described the data well by simulating data from it and comparing the moments (mean, variance, skewness, and kurtosis) of simulated and real data.

**Flowering and fruit production** We modeled shrub reproductive status (vegetative or flowering) in year  $t$  as a Bernoulli random variable with three candidate models for flowering probability. These included smooth terms for current size (in year  $t$ ) only (1), size and weighted density (3), and both smooth terms plus an interaction between size and weighted density. We modeled the reproductive output of flowering plants (the sum

280 of flowerbuds, open flowers, and fruits) in year  $t$  as a negative binomial random variable.  
281 There were three candidate models for mean reproductive output that corresponded to  
282 the same three candidates for flowering probability.

283 **Recruitment and recruit size** We modeled seedling recruitment in each transect  
284 window as a binomial random variable given the number of total seeds produced in that  
285 window in the preceding year. There were two candidate models, with and without  
286 an influence of weighted density on the per-seed recruitment probability. To estimate  
287 window-level seed production, we used the best-fit models for flowering and fruit produc-  
288 tion and applied this to all plants in each window that we observed in our initial density  
289 surveys. We assume that recruits come from the previous year's seeds and not from a  
290 long-lived soil seed bank.

291 We modeled recruit size as a Gaussian-distributed random variable and fit four can-  
292 didate models including an influence of weighted density on mean, variance, both, and  
293 neither.

## 294 **Density-dependent IPM**

295 The size- and density-dependent statistical models comprised the sub-models of a density  
296 dependent Integral Projection Model (IPM) that we used to evaluate how the shrub  
297 population growth rate responded to con-specific density; we present this non-spatial  
298 model before layering on the spatial dynamics generated by seed dispersal. A basic  
299 density-independent IPM predicts the number of individuals of size  $x'$  at time  $t + 1$   
300 ( $n(x', t + 1)$ ) based on a demographic projection kernel ( $K_{dem}$ ) that gives the rates of  
301 transition from sizes  $x$  to  $x'$  from times  $t$  to  $t+1$  and is integrated over the size distribution  
302 from the minimum ( $L$ ) to maximum ( $U$ ) sizes. In a density-dependent IPM, components

of the projection kernel may respond to population abundance and structure:

$$n(x', t + 1) = \int_L^U K_{dem}(x', x, \tilde{n}(t)) n(x, t) dx \quad (1)$$

Here,  $\tilde{n}(t)$  is some function of population structure  $n(x, t)$  such as the total density of conspecifics ( $\tilde{n}(t) = \int n(x, t) dx$ ) or, as in our case, total density weighted by size ( $\tilde{n}(t) = \int x n(x, t) dx$ ). For simplicity, in the analyses that follow we do not model density as a dynamic state variable; instead, we treat density as a static covariate ( $\tilde{n}(t) = \tilde{n}$ ) and evaluate the IPM at a range of density values. As in our statistical modeling, the size variable of the IPM ( $x, x'$ ) was  $\log(\text{cm}^3)$ .

For our model, the size- and density-dependent demographic transitions captured by the projection kernel include growth or shrinkage ( $g$ ) from size  $x$  to  $x'$  conditioned on survival ( $s$ ) at size  $x$  (combined growth-survival function  $G(x', x, \tilde{n}) = g(x', x, \tilde{n})s(x, \tilde{n})$ ), and the production of new size- $x'$  individuals from size- $x$  parents ( $Q(x', x, \tilde{n})$ ). Reproduction reflects the probability of flowering at size  $x$  ( $p$ ), the number of seeds produced by flowering plants ( $d$ ), the per-seed probability of recruitment ( $r$ ), and the size distribution of recruits ( $c$ ). Collectively, the rate at which  $x$ -sized individuals produce  $x'$ -sized individuals at density  $\tilde{n}$  is given by the combined reproduction-recruitment function  $Q(x', x, \tilde{n}) = p(x, \tilde{n})d(x, \tilde{n})r(\tilde{n})c(x', \tilde{n})$ . Thus, we can express the projection kernel as:

$$K_{dem}(x', x, \tilde{n}) = G(x', x, \tilde{n}) + Q(x', x, \tilde{n}) \quad (2)$$

For analysis, we evaluated the IPM kernel over a range of local densities from the minimum to the maximum of weighted density values from the 5-meter windows ( $0 \leq \tilde{n} \leq \tilde{n}_{max}$ ). At each density level, we discretized the IPM kernel into a  $200 \times 200$  approximating matrix and calculated the asymptotic growth rate  $\lambda(\tilde{n})$  as its leading eigenvalue. We extended the lower ( $L$ ) and upper ( $U$ ) integration limits to avoid unintentional “eviction” using the floor-and-ceiling method (Williams et al., 2012).

327 We sought to characterize the shape of density dependence: whether fitness declined  
 328 monotonically or not with increasing density. We quantified uncertainty in the density-  
 329 dependent growth rate  $\lambda(\tilde{n})$  by bootstrapping our data. For each bootstrap, we randomly  
 330 sampled 75% of our demographic data, re-ran the statistical modeling and model selec-  
 331 tion, and used the top vital rate models to generate  $\lambda(\tilde{n})$  for that data subset. We  
 332 repeated this procedure for 500 bootstrap replicates.

### 333 **Dispersal modelling**

334 **WALD dispersal model** Dispersal kernels were calculated using the WALD, or Wald  
 335 analytical long-distance dispersal, model that uses a mechanistic approach to predict  
 336 dispersal patterns of plant propagules by wind. The WALD model, which is based in fluid  
 337 dynamics, can serve as a good approximation of empirically-determined dispersal kernels  
 338 (Katul et al., 2005; Skarpaas and Shea, 2007) and may be used when direct observations  
 339 of dispersal are not available. Under the assumptions that wind turbulence is low, wind  
 340 flow is vertically homogenous, and terminal velocity is achieved immediately upon seed  
 341 release, the WALD model simplifies a Lagrangian stochastic model to create a dispersal  
 342 kernel that estimates the likelihood a propagule will travel a given distance (Katul et al.,  
 343 2005). Our dispersal kernel takes the form of the inverse Gaussian distribution

$$344 \quad p(r) = \left( \frac{\lambda'}{2\pi r^3} \right)^{\frac{1}{2}} \exp \left[ -\frac{\lambda'(r - \mu')^2}{2\mu'^2 r} \right] \quad (3)$$

345 that is a **slight adaptation**<sup>4</sup> from equation 5b in Katul et al. (2005), using  $r$  to denote  
 346 dispersal distance. Here,  $\lambda'$  is the location parameter and  $\mu'$  is the scale parameter, which  
 347 depend on environmental and plant-specific properties of the study system. (We use  $\lambda'$   
 348 for consistency with notation in related papers, but  $\lambda'$  the dispersal location parameter  
 349 should not be confused with  $\lambda$  the geometric growth rate.) The location and scale  
 350 parameters are defined as  $\lambda' = (H/\sigma)^2$  and  $\mu' = HU/F$ ; these are functions of the height

---

<sup>4</sup>*unclear what this refers to*



351  $H$  of seed release, wind speed  $U$  at seed release height, seed terminal velocity  $F$ , and  
 352 the turbulent flow parameter  $\sigma$  that depends on both wind speed and local vegetation  
 353 roughness. We parameterized the WALD dispersal kernel using windspeed data from  
 354 the SEV-LTER weather station nearest our study site (Moore and Hall, 2022) and seed  
 355 terminal velocity data from laboratory-based seed-drop experiments (Appendix A). We  
 356 integrated the dispersal kernel over observed variation in wind speeds, seed terminal  
 357 velocity, and release height within the height of a shrub. Therefore the dispersal kernel  
 358 for a shrub of height  $U$  was given by:

$$359 \quad K_{disp} = \iiint p(F)p(U)p(z)p(r) dF dU dz \quad (4)$$

360 and  $p(F)$  and  $p(U)$  are the PDFs of the terminal velocity  $F$  and wind speed  $U$ ,  
 361 respectively, and  $p(z)$  is the uniform distribution from the minimum seed release height  
 362 ( $0.15m$ , the height at which grass cover interferes with wind dispersal) to  $H$ . Methods for  
 363 our seed data collection and technical details of dispersal kernel modeling are provided  
 364 in Appendix A.

### 365 **Spatial integral projection model**

366 We used a spatial integral projection model to piece together seed dispersal and density-  
 367 dependent demography, and generate predictions for the rate of shrub expansion that  
 368 results from this combination of local and spatial processes. The spatially explicit model  
 369 builds upon the non-spatial model (Eq. 1) and adds a spatial variable  $(z, z')$  such  
 370 that demographic transitions occur across both time and space according to a combined  
 371 demography-dispersal kernel  $\tilde{K}$ :

$$372 \quad n(xt, zt, t + 1) = \int_{-\infty}^{+\infty} \int_L^U \tilde{K}(xt, x, zt, z, \tilde{n}(z, t)) n(x, z, t) dx dz \quad (5)$$

373 Here,  $\tilde{K}(xt, x, zt, z, \tilde{n}(z, t))$  describes the transition from size  $x$  and location  $z$  to size

374  $x'$  and location  $z'$  given density  $\tilde{n}(z, t)$  at starting location  $z$ . As before,  $\tilde{n}$  is a function  
 375 of population structure – in our model, weighted local density – but here integrated  
 376 over an explicit competitive “neighborhood”:  $\tilde{n}(z, t) = \int_{z-h}^{z+h} \int_L^U x n(x, z, t) dx dz$  where  $h$   
 377 represents neighborhood size in the units of  $z$ . The demography-dispersal kernel  $\tilde{K}$  is  
 378 given by the sum of two parts, one that describes reproduction coupled with dispersal of  
 379 propagules, and another that describes growth and survival of non-dispersing individuals:

$$380 \quad \tilde{K}(x', x, z', z, \tilde{n}(z, t)) = K_{disp}(z' - z)Q(x', x, \tilde{n}) + \delta(z' - z)G(x', x, \tilde{n}) \quad (6)$$

381 Here, regeneration function  $Q$  and growth-survival function  $G$  correspond to Eq. 2,  
 382 dispersal kernel  $K_{disp}$  corresponds to Eq. , and the Dirac delta function is a probability  
 383 distribution with all mass at zero, which prevents movement. Following standard as-  
 384 sumptions for integro-difference equations, we assume that space is one-dimensional and  
 385 homogeneous, such that demographic transitions do not depend on location (or, more  
 386 precisely, that they depend on location only through spatial variation in density) and  
 387 the probability of dispersing from location  $z$  to  $z'$  depends only on the absolute distance  
 388 between them.

389 Under many conditions, models of this form generate traveling waves, and we are  
 390 particularly interested in the velocity ( $m/yr$ ) of this wave. Methods to estimate this  
 391 velocity depend strongly on how demography responds to density. If fitness is maximized  
 392 at some density  $\tilde{n} > 0$  then the wave is pushed and wave velocity can only be estimated  
 393 through numerical simulation. However, if fitness is maximized at  $\tilde{n} = 0$  then the wave  
 394 is pulled and an upper bound on its asymptotic velocity can be calculated analytically,  
 395 following Neubert and Caswell (2000) and Jongejans et al. (2011), as

$$396 \quad c^* = \min_{s>0} \left[ \frac{1}{s} \ln(\rho_s) \right] \quad (7)$$

397 where  $s$  is a wave shape parameter and  $\rho_s$  is the dominant eigenvalue of the kernel

398  $H_s(x', x)$ . Corresponding to Eq. 6 and assuming  $\tilde{n} = 0$ ,  $H_s$  is composed of

$$399 \quad H_s(x', x) = M(s, x)Q(x', x) + G(x', x) \quad (8)$$

400 where  $M(s, x)$  is the moment-generating function for the dispersal kernel associated  
 401 with size  $x$ . This formulation of the model assumes that the dispersal kernel depends  
 402 only on maternal size  $x$  and not offspring size  $x'$ . To estimate  $M(s, x)$  we simulated  
 403  $N = 10000$  dispersal events ( $r$ ) for each size  $x$  and marginalized these over one spatial  
 404 dimension as in Lewis et al. (2006). We then evaluated the empirical moment-generating  
 405 function for each size  $x$ :  $M(s) = \frac{1}{N} \sum_{i=1}^N e^{sr}$ .

406 Estimates of wavespeed were bootstrapped for a total of 1000 replicates. Each boot-  
 407 strap replicate recreated size- and density-dependent demographic models using 50%  
 408 resampling on the original demographic data, and recreated dispersal kernels also us-  
 409 ing 50% resampling on the wind speeds and seed terminal velocities. Model selection  
 410 for demographic vital rates was re-run for each bootstrap replicate, so this approach  
 411 incorporates both parameter and model uncertainty.

## 412 **Encroachment re-surveys**

413 We recorded shrub percent cover along two permanent 1000-m transects that spanned  
 414 the shrub-grass ecotone, from high to low to near-zero shrub density. These surveys were  
 415 conducted in summer 2001 and again in summer 2013 to document change in creosotebush  
 416 abundance and spatial extent. At every 10 meters, shrub cover was recorded in nine cover  
 417 classes (<1%, 1–4%, 5–10%, 10–25%, 25–33%, 33–50%, 50–75%, 75–95%, >95%). For  
 418 visualization, we show midpoint values of these cover classes at each meter location for  
 419 both transects and years.

## 420 **Results**

### 421 **Size and density dependent demography**

422 Demographic data from naturally occurring and transplanted individuals revealed strong  
423 size- and density-dependence in demographic vital rates. For most sizes and vital rates,  
424 local density had negative demographic effects. Statistical support for size- and density-  
425 dependence is provided in Table XX, which provides AIC rankings for candidate models  
426 based on the completed (not bootstrapped) data set.

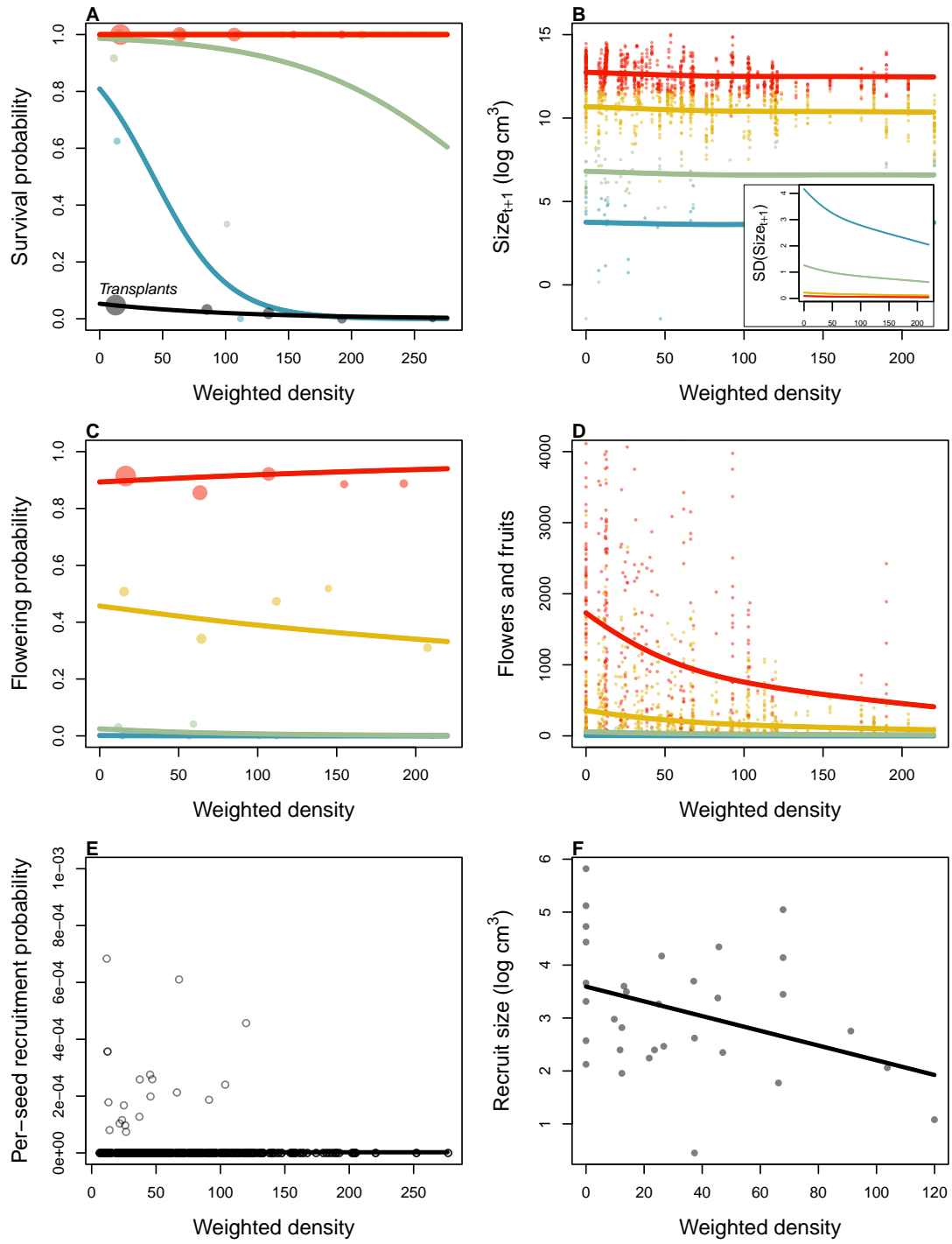


Figure 2: Size- and density-dependence in demographic vital rates. **A** Probability of survival from natural population census and transplant experiment (black line), **B** Mean and variance (inset) of size conditional on previous size, **C** Probability of flowering, **D** Flower and fruit production, **E** Probability of recruitment per seed, **F** Recruit size. In **A–E**, colored lines indicate four size groups (red is largest, blue is smallest), discretized for data visualization only. In all panel, weighted density is the sum of all plant sizes  $\log(\text{cm}^3)$  within the same 5-m window as the census individual.

427 **Survival** Among naturally occurring plants, survival of large, established individuals  
428 was very high (Fig. 2A). We observed relatively few mortality events and nearly all of  
429 these were among new recruits. The probability of survival at these small sizes declined  
430 with increasing density. Survival of transplants was very low, lower even than survival  
431 of similarly-sized, naturally occurring recruits (Fig. 2B). However, the transplant results  
432 support the general pattern of negative density dependence in survival. Among the 20  
433 survivors, 15 of them occurred in transect windows below the median of weighted shrub  
434 density.

435       SHORT PARAGRAPH SUMMARIZING SMALLER-SCALE ANALYSIS IN AP-  
436 PENDIX.

437 **Growth** Current size was strongly predictive of future size, as expected, and there  
438 was weak negative density dependence in mean future size conditioned on current size  
439 (Fig. 2C). However, there was a stronger signal of density dependence in the variance of  
440 future size (Fig. 2C, inset). Plants at low density exhibited greater variance in growth  
441 trajectories and this was especially true at the smallest sizes. Thus, large increases in  
442 the size of new recruits were most likely to occur under low-density conditions.

443 **Flowering and fruit production** Flowering probability was strongly size-dependent  
444 and and very weakly sensitive to local density (Fig. 2D). However, fertility of flowering  
445 plants was strongly negative density dependent, with greatest flower and fruit production  
446 by the largest plants at the lowest densities, and vice versa (Fig. 2E).

447 **Recruitment and recruit size** We observed 32 natural recruitment events along our  
448 transects during the study years and our estimate recruitment rate, given total expected  
449 seed production in each window preceding the recruitment year, was very low ( $2.47 \times 10^{-6}$ ,  
450 2F). While most recruitment events occurred at low density, this is also where most seed  
451 production was concentrated (Fig. 2E) and low-density windows were over-represented

relative to high density. For these reasons we were more likely to observe recruitment events at low density. Controlling for sampling effort and seed production, the statistical models indicated that our data were most consistent with a constant, density-independent recruitment rate (Table XX). However, the mean size of new recruits declined significantly with local density (Fig. 2F).

**Population growth rate** As expected based on the vital rate results, the asymptotic population growth rate  $\lambda$  declined monotonically with density (Fig. 3). This was true across all bootstrap replicates, indicating high certainty that shrub fitness is maximized at zero density and thus that the expansion wave is “pulled”. Mean growth rate at low density was 3% per year, with bootstrap uncertainty spanning 1–6%. At high density in the core of the expansion wave, population growth rates approached  $\lambda = 1$ , indicating population stasis driven by near-perfect survival and extremely rare recruitment.

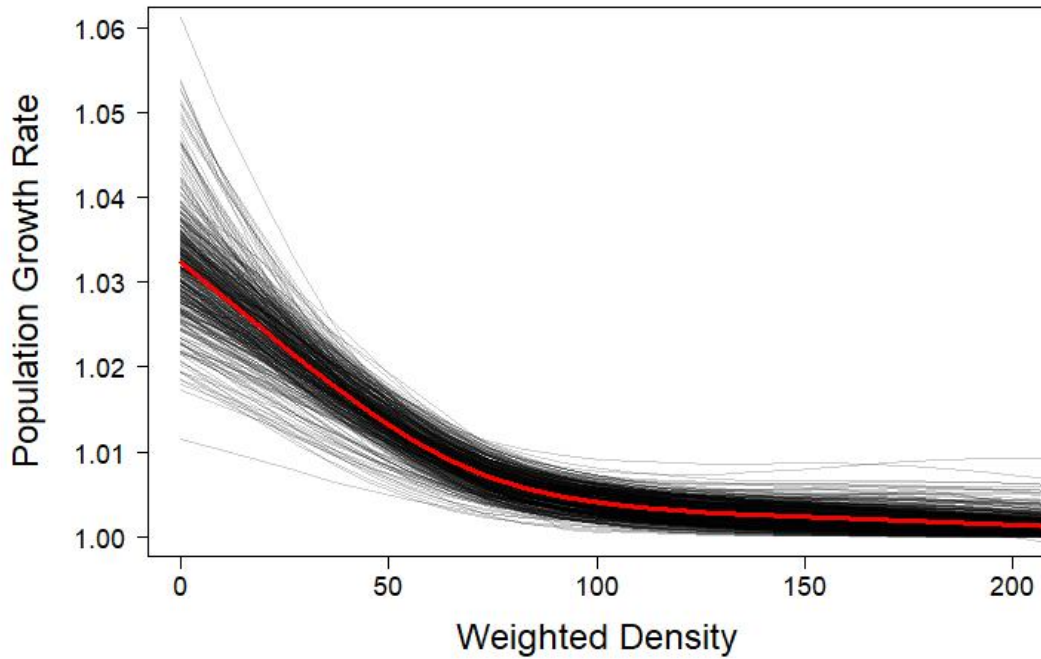


Figure 3: Density dependence in the asymptotic population growth rate ( $\lambda$ ). Lines show bootstrap replicates sub-sampled from the full demographic data set. Weighted deighted density is the sum of all plant sizes  $\log(cm^3)$  within 5-m windows.

## Seed dispersal

As the speed of encroachment is quite limited, so is the extent of wind dispersal. Long distance dispersal events, while more common for taller shrubs than their shorter counterparts, are still uncommon overall. For the tallest shrub height of 1.98 m, only 0.32% of propagules exceed a dispersal distance of 5 m, and 0.02% exceed 10 m. At 1 m, or approximately half the tallest shrub height, long distance dispersal is even less likely, with 0.0046% of propagules exceeding a dispersal distance of 5 m and 0.0009% exceeding 10 m. Given that the median shrub height is only 0.64 m, the occurrence of long-distance wind dispersal in most of the shrub population is highly improbable, and the few instances in which it occurs will only be limited to the tallest shrubs. Thus, as Figure 4 demonstrates,



474 shorter dispersal distances dominate; even for the tallest shrub, 81% of seeds fall within  
 475 only a metre of the plant, and this percentage increases as shrub height decreases. Dis-  
 476 persal kernels have their highest probability density at dispersal distances between 2 and  
 477 8 cm from the shrub; here, as shrub height increases, the most probable dispersal dis-  
 478 tance slightly increases while maximum probability density decreases. Regardless of the  
 479 shrub height, most dispersal will occur very close to the plant, though increases in shrub  
 480 height dramatically increase the likelihood of dispersal at longer distances. It is clear  
 481 that the shape of the height-dependent dispersal kernel  $K(r)$  varies greatly among the  
 482 shrub population given the large range of shrub heights observed; shrubs at lower heights  
 483 have more slender kernels with most of the seeds dispersing closer to the plant, while  
 484 taller shrubs have kernels with much fatter tails and are more capable of longer-distance  
 485 dispersal.

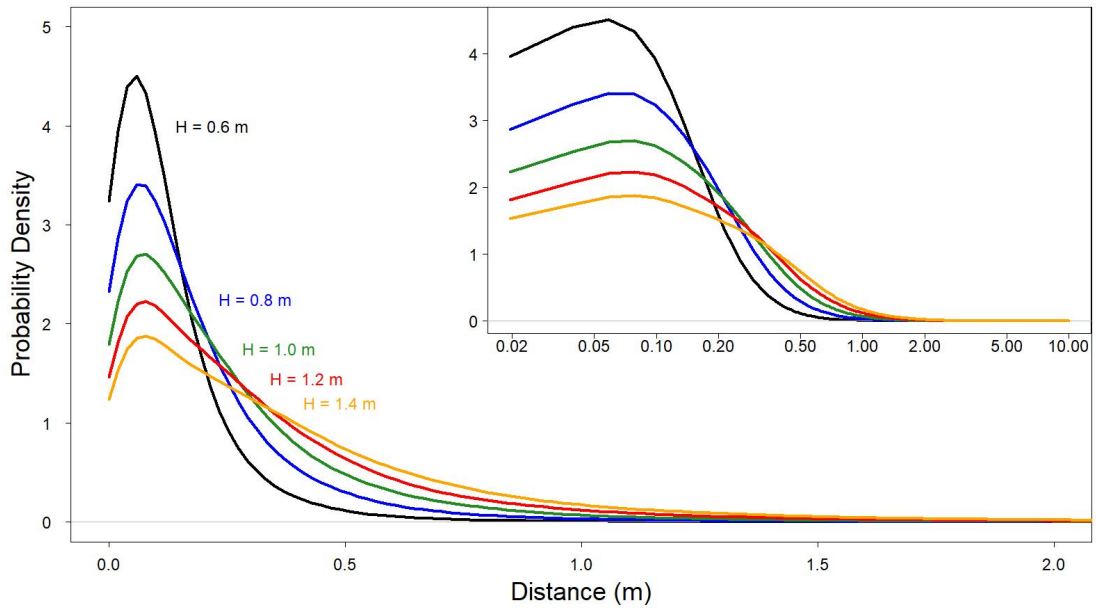


Figure 4: Dispersal kernels, with each colour representing a selected shrub height. The inset plot is the same as the large plot, though with a logarithmic x-axis to more easily show differences in dispersal probability at smaller distances.

## Expansion speed

The speed of encroachment at the study site as estimated by the SIPM is rather slow; as can be seen in Figure 5, the low-density wavefront moves at approximately 0.5 cm/yr under normal conditions and at 1 cm/yr under the best seedling survival conditions observed in the dataset. These improved conditions were observed due to above-average rainfall that occurred after greenhouse-grown seedlings were transplanted to the site. Population growth in this low-density region of the moving wave is also low, with a geometric growth rate of  $\lambda \approx 1.006$  and even lower rates of growth the higher-density regions behind; in the higher-survival scenario the maximum rate increases to  $\lambda \approx 1.013$ , with growth still decreasing as density increases. For both scenarios, the decrease in population growth rate with increasing density was monotonic across the range of observed standardised densities, as is shown in Figure 5. This suggests that an Allee effect is likely not present in this population, as the highest rate of population growth is found at the lowest density vanguard of the encroaching population. Thus, the conditions necessary for equation 9 to be valid are satisfied, and these wavespeeds are applicable for a pulled-wave scenario in which no Allee effects are present.

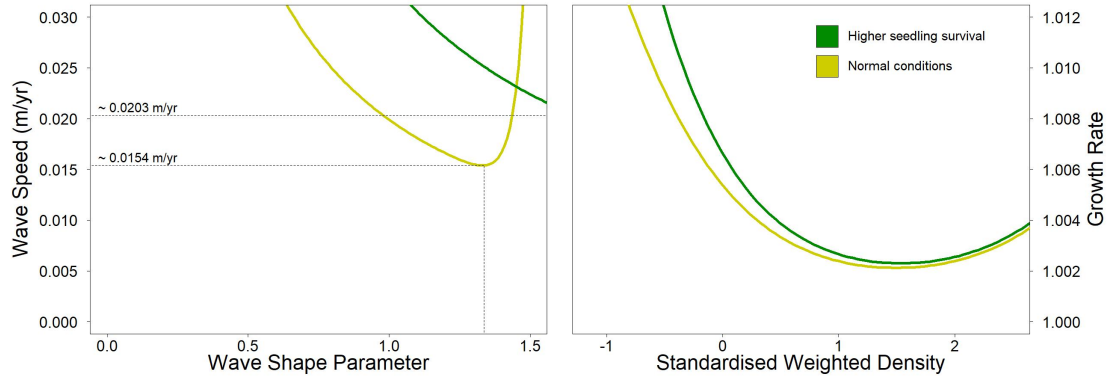


Figure 5: Estimated encroachment wave speeds (left) and geometric rates of population growth (right) for higher post-rainfall seedling survival and normal conditions.

## 502 Transect re-surveys

503 Re-surveys along two permanent transects revealed virtually no change the in the creosote  
504 expansion wave over 12 years (Fig. 6). There were local changes in percent cover: on  
505 average cover increased by XX% between surveys. However, there was no clear indication  
506 that the leading edge of the creosote shrubland has advanced (the modest right-ward shift  
507 on both transects is within the range of measurement error).

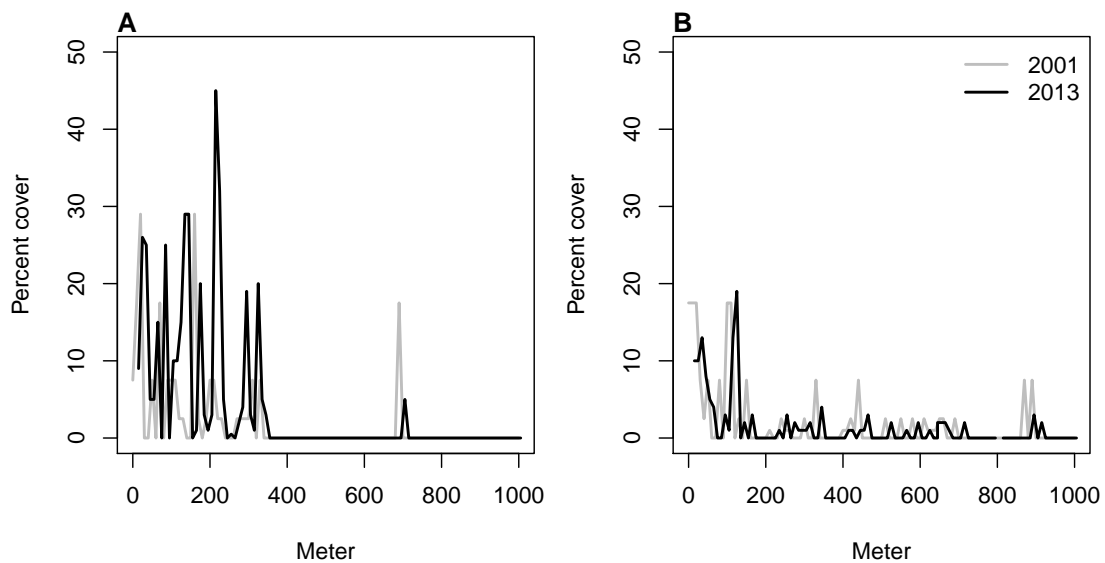


Figure 6: Re-surveys of shrub cover along two permanent trasects (A,B) surveyed in 2001 and 2013.

## 508 Discussion

509 The slow movement of the encroaching creosotebush wave at the Sevilleta LTER site  
510 can likely be contributed to a combination of three factors: short dispersal distances  
511 with extremely limited long-distance dispersal events, very low probability of recruit-  
512 ment from seed, and high seedling mortality. These three barriers, when combined, form  
513 a formidable challenge to the establishment of new shrubs at the low-density front of  
514 the wave. First, a seed must travel far enough to avoid competition with the parent

shrub, which is unlikely given the dispersal kernels shown in Figure 2. Even if the seed manages to be dispersed this far, its chances of becoming a seedling are low. Caching and consumption by seed-eaters such as a variety of seed-harvesting ants (Whitford, 1978; Whitford et al., 1980; Lei, 1999) and the kangaroo rat *Dipodomys merriami* (Chew and Chew, 1970) decreases the amount of seeds available for germination. However, reduction in germination caused by destruction of seeds may be partly mitigated by the more favourable germination conditions that these seeds can experience when cached underground (Chew and Chew, 1970). Many of the remaining seeds will still fail to germinate, and in the unlikely event that germination does occur, seedlings will likely die given the high rates of mortality observed in smaller shrubs. Such high rates of creosotebush seedling mortality have been observed in other studies as well (Boyd and Brum, 1983; Bowers et al., 2004), probably due to a combination of herbivory, competition, and abiotic stresses.

However, as low as they are, the wavespeed estimates given in this paper are still conservative estimates for reasons mostly related to dispersal. First, it is important to note that the dispersal kernels used here, while they account for variation in factors such as wind speed and terminal velocity, may underestimate the distances that shrub propagules travel. Because the WALD model assumes that terminal velocity is reached immediately upon seed release, seeds in the estimate thus take a shorter time to fall and have less time to be transported by wind, and the true frequency of long-distance dispersal events may thus be greater than what is estimated here. Second, dispersal at the study site could occur through additional mechanisms other than wind. For example, secondary dispersal through runoff from significant rainfall events can transport seeds (Thompson et al., 2014), and given that long-distance dispersal by bird and subsequent species divergence is thought to be responsible for creosotebush being in North America in the first place (Wells and Hunziker, 1976), short-distance dispersal by other animals at the study site likely occurs. As mentioned above, seeds are transported by seed-

542 harvesting ants and granivorous mammals, where they are often stored in caches that  
543 can be appreciable distances from the parent shrubs. Whether transportation occurs via  
544 ant or rodent, creosotebush seeds can be moved significantly further than wind alone  
545 can, though many of these seeds are eventually consumed.

546 Despite the more conservative estimates our model yields, the estimated rate of dis-  
547 persal in creosotebush populations at the Sevilleta National Wildlife Refuge is consistent  
548 with observations from the past 50-60 years, as creosotebush expansion during this time  
549 has been minimal (Moreno-de las Heras et al., 2016). However, it cannot explain the  
550 long-term increases in creosotebush cover at the study site, as total encroachment over  
551 the past 150 years is much greater than what would be expected given the encroachment  
552 rates derived by our models. Such a discrepancy is likely due to much of the expansion  
553 occurring in an episodic fashion, with short times during which rapid encroachment oc-  
554 curs due to favourable environmental conditions. This could be due in part to seedling  
555 recruitment, which is a factor that strongly limits creosotebush expansion, being rare  
556 and episodic. For example, Allen et al. (2008) estimate that a major recruitment event  
557 occurred at this site in the 1950s, which is supported by photographic evidence from  
558 Milne et al. (2003) of a drought-driven expansion during this time. Moreno-de las Heras  
559 et al. (2016) estimate that after this expansion, several smaller creosotebush recruitment  
560 events occurred in decadal episodes. However, such events can be highly localised and  
561 may not necessarily occur at the low-density front of encroachment, which could explain  
562 how these recruitment events can still coexist with lack of encroachment in the recent  
563 past.

564 Overall, our observations and model highlight three aspects of creosotebush encroach-  
565 ment that should be the focus of future studies seeking to obtain better estimates of  
566 encroachment rates. First, negative density dependence in survival, growth, and repro-  
567 duction is demonstrated, along with size dependence. The clear dependence on size and  
568 conspecific density suggests that they both should be considered when estimating cre-

osotebush expansion and quantifying the demographic variation that contributes to it. Second, wind dispersal in these shrubs is quite limited; though the dispersal kernels seen here are typical in the sense that they are characterised by high near-plant dispersal and exceptionally low long-distance dispersal, the scale across which such dispersal occurs is small, with most seeds landing within only 1 m of the shrub. Wind dispersal alone may be an underestimate of the true amount of dispersal occurring, and future work should seek to incorporate the effects of dispersal by runoff and animals so that a more representative model of total dispersal can be obtained. Finally, encroachment is slow or even stagnates, but only most of the time. Though our encroachment speed estimates are representative of creosotebush populations for most years, the significant expansion seen over larger time scales suggests that there is episodic expansion in other years; while our model is consistent with the recent stagnation in creosotebush encroachment at the Sevilleta LTER site, a model that also includes interannual variability in factors such as survival and recruitment would be able to better account for instances of episodic population expansion that are characteristic of this location.

## Acknowledgements

## Author contributions

## Data accessibility

## References

- Allen, A., W. Pockman, C. Restrepo, and B. Milne. 2008. Allometry, growth and population regulation of the desert shrub *Larrea tridentata*. *Functional Ecology* pages 197–204.
- Bowers, J. E., R. M. Turner, and T. L. Burgess. 2004. Temporal and spatial patterns in

592 emergence and early survival of perennial plants in the Sonoran Desert. *Plant Ecology*  
593 **172**:107–119.

594 Boyd, R. S., and G. D. Brum. 1983. Postdispersal reproductive biology of a Mojave Desert  
595 population of *Larrea tridentata* (Zygophyllaceae). *American Midland Naturalist* pages  
596 25–36.

597 Brandt, J. S., M. A. Haynes, T. Kuemmerle, D. M. Waller, and V. C. Radeloff. 2013.  
598 Regime shift on the roof of the world: Alpine meadows converting to shrublands in  
599 the southern Himalayas. *Biological Conservation* **158**:116–127.

600 Buffington, L. C., and C. H. Herbel. 1965. Vegetational changes on a semidesert grassland  
601 range from 1858 to 1963. *Ecological monographs* **35**:139–164.

602 Bullock, J. M., S. M. White, C. Prudhomme, C. Tansey, R. Perea, and D. A. Hooftman.  
603 2012. Modelling spread of British wind-dispersed plants under future wind speeds in  
604 a changing climate. *Journal of Ecology* **100**:104–115.

605 Cabral, A., J. De Miguel, A. Rescia, M. Schmitz, and F. Pineda. 2003. Shrub encroach-  
606 ment in Argentinean savannas. *Journal of Vegetation Science* **14**:145–152.

607 Chew, R. M., and A. E. Chew. 1970. Energy relationships of the mammals of a desert  
608 shrub (*Larrea tridentata*) community. *Ecological Monographs* pages 2–21.

609 D’Odorico, P., J. D. Fuentes, W. T. Pockman, S. L. Collins, Y. He, J. S. Medeiros,  
610 S. DeWekker, and M. E. Litvak. 2010. Positive feedback between microclimate and  
611 shrub encroachment in the northern Chihuahuan desert. *Ecosphere* **1**:1–11.

612 D’Odorico, P., G. S. Okin, and B. T. Bestelmeyer. 2012. A synthetic review of feedbacks  
613 and drivers of shrub encroachment in arid grasslands. *Ecohydrology* **5**:520–530.

614 Gandhi, S. R., E. A. Yurtsev, K. S. Korolev, and J. Gore. 2016. Range expansions  
615 transition from pulled to pushed waves as growth becomes more cooperative in an

616 experimental microbial population. *Proceedings of the National Academy of Sciences*  
617 **113**:6922–6927.

618 Gardner, J. L. 1951. Vegetation of the creosotebush area of the Rio Grande Valley in  
619 New Mexico. *Ecological Monographs* **21**:379–403.

620 Gibbens, R., R. McNeely, K. Havstad, R. Beck, and B. Nolen. 2005. Vegetation changes  
621 in the Jornada Basin from 1858 to 1998. *Journal of Arid Environments* **61**:651–668.

622 Goslee, S., K. Havstad, D. Peters, A. Rango, and W. Schlesinger. 2003. High-resolution  
623 images reveal rate and pattern of shrub encroachment over six decades in New Mexico,  
624 USA. *Journal of Arid Environments* **54**:755–767.

625 Grover, H. D., and H. B. Musick. 1990. Shrubland encroachment in southern New Mexico,  
626 USA: an analysis of desertification processes in the American Southwest. *Climatic*  
627 *change* **17**:305–330.

628 Hsieh, C.-I., and G. G. Katul. 1997. Dissipation methods, Taylor’s hypothesis, and  
629 stability correction functions in the atmospheric surface layer. *Journal of Geophysical*  
630 *Research: Atmospheres* **102**:16391–16405.

631 Huang, H., L. D. Anderegg, T. E. Dawson, S. Mote, and P. D’Odorico. 2020. Crit-  
632 ical transition to woody plant dominance through microclimate feedbacks in North  
633 American coastal ecosystems. *Ecology* **101**:e03107.

634 Jongejans, E., K. Shea, O. Skarpaas, D. Kelly, and S. P. Ellner. 2011. Importance of  
635 individual and environmental variation for invasive species spread: a spatial integral  
636 projection model. *Ecology* **92**:86–97.

637 Katul, G., A. Porporato, R. Nathan, M. Siqueira, M. Soons, D. Poggi, H. Horn, and  
638 S. A. Levin. 2005. Mechanistic analytical models for long-distance seed dispersal by  
639 wind. *The American Naturalist* **166**:368–381.



- 640 Keitt, T. H., M. A. Lewis, and R. D. Holt. 2001. Allee effects, invasion pinning, and  
641 species' borders. *The American Naturalist* **157**:203–216.
- 642 Kelleway, J. J., K. Cavanaugh, K. Rogers, I. C. Feller, E. Ens, C. Doughty, and N. Sain-  
643 tilan. 2017. Review of the ecosystem service implications of mangrove encroachment  
644 into salt marshes. *Global Change Biology* **23**:3967–3983.
- 645 Knapp, A. K., J. M. Briggs, S. L. Collins, S. R. Archer, M. S. BRET-HARTE, B. E.  
646 Ewers, D. P. Peters, D. R. Young, G. R. Shaver, E. Pendall, et al. 2008. Shrub  
647 encroachment in North American grasslands: shifts in growth form dominance rapidly  
648 alters control of ecosystem carbon inputs. *Global Change Biology* **14**:615–623.
- 649 Kot, M., M. A. Lewis, and P. van den Driessche. 1996. Dispersal data and the spread of  
650 invading organisms. *Ecology* **77**:2027–2042.
- 651 Lei, S. A. 1999. Ecological impacts of *Pogonomyrmex* on woody vegetation of a *Larrea*-  
652 *Ambrosia* shrubland. *The Great Basin Naturalist* pages 281–284.
- 653 Lewis, M., and P. Kareiva. 1993. Allee dynamics and the spread of invading organisms.  
654 *Theoretical Population Biology* **43**:141–158.
- 655 Lewis, M. A., M. G. Neubert, H. Caswell, J. S. Clark, and K. Shea, 2006. A guide  
656 to calculating discrete-time invasion rates from data. Pages 169–192 *in* *Conceptual*  
657 *ecology and invasion biology: reciprocal approaches to nature*. Springer.
- 658 Mabry, T. J., J. H. Hunziker, D. Difeo Jr, et al. 1978. Creosote bush: biology and  
659 chemistry of *Larrea* in New World deserts. Dowden, Hutchinson & Ross, Inc.
- 660 Maddox, J. C., and S. Carlquist. 1985. Wind dispersal in Californian desert plants:  
661 experimental studies and conceptual considerations. *Aliso: A Journal of Systematic*  
662 *and Evolutionary Botany* **11**:77–96.

- 663 Milne, B. T., D. I. Moore, J. L. Betancourt, J. A. Parks, T. W. Swetnam, R. R. Par-  
664 menter, and W. T. Pockman. 2003. Multidecadal drought cycles in south-central New  
665 Mexico: Patterns and consequences. Oxford University Press: New York, NY.
- 666 Moore, D., and K. Hall, 2022. Meteorology Data from the Sevilleta  
667 National Wildlife Refuge, New Mexico. Environmental Data Initiative.  
668 <https://doi.org/10.6073/pasta/d56307b398e28137dabaa6994f0f5f92>.
- 669 Moreno-de las Heras, M., L. Turnbull, and J. Wainwright. 2016. Seed-bank structure  
670 and plant-recruitment conditions regulate the dynamics of a grassland-shrubland Chi-  
671 huahuan ecotone. *Ecology* **97**:2303–2318.
- 672 Mugasi, S., E. Sabiiti, and B. Tayebwa. 2000. The economic implications of bush  
673 encroachment on livestock farming in rangelands of Uganda. *African Journal of Range  
674 and Forage Science* **17**:64–69.
- 675 Nathan, R., G. G. Katul, G. Bohrer, A. Kuparinen, M. B. Soons, S. E. Thompson,  
676 A. Trakhtenbrot, and H. S. Horn. 2011. Mechanistic models of seed dispersal by wind.  
677 *Theoretical Ecology* **4**:113–132.
- 678 Neubert, M. G., and H. Caswell. 2000. Demography and dispersal: calculation and  
679 sensitivity analysis of invasion speed for structured populations. *Ecology* **81**:1613–  
680 1628.
- 681 Oba, G., E. Post, P. Syvertsen, and N. Stenseth. 2000. Bush cover and range condition  
682 assessments in relation to landscape and grazing in southern Ethiopia. *Landscape  
683 ecology* **15**:535–546.
- 684 Pan, S., and G. Lin. 2012. Invasion traveling wave solutions of a competitive system  
685 with dispersal. *Boundary Value Problems* **2012**:120.

- 686 Parizek, B., C. M. Rostagno, and R. Sottini. 2002. Soil erosion as affected by shrub  
687 encroachment in northeastern Patagonia. *Rangeland Ecology & Management/Journal*  
688 *of Range Management Archives* **55**:43–48.
- 689 Peters, D. P., and J. Yao. 2012. Long-term experimental loss of foundation species:  
690 consequences for dynamics at ecotones across heterogeneous landscapes. *Ecosphere*  
691 **3**:1–23.
- 692 Ratajczak, Z., J. B. Nippert, and S. L. Collins. 2012. Woody encroachment decreases  
693 diversity across North American grasslands and savannas. *Ecology* **93**:697–703.
- 694 Raupach, M. 1994. Simplified expressions for vegetation roughness length and zero-  
695 plane displacement as functions of canopy height and area index. *Boundary-Layer*  
696 *Meteorology* **71**:211–216.
- 697 Ravi, S., P. D’Odorico, S. L. Collins, and T. E. Huxman. 2009. Can biological invasions  
698 induce desertification? *The New Phytologist* **181**:512–515.
- 699 Reed, M., L. Stringer, A. Dougill, J. Perkins, J. Athopheng, K. Mulale, and N. Favretto.  
700 2015. Reorienting land degradation towards sustainable land management: Linking  
701 sustainable livelihoods with ecosystem services in rangeland systems. *Journal of envi-*  
702 *ronmental management* **151**:472–485.
- 703 Reynolds, J. F., R. A. Virginia, P. R. Kemp, A. G. De Soyza, and D. C. Tremmel. 1999.  
704 Impact of drought on desert shrubs: effects of seasonality and degree of resource island  
705 development. *Ecological Monographs* **69**:69–106.
- 706 Roques, K., T. O’connor, and A. R. Watkinson. 2001. Dynamics of shrub encroach-  
707 ment in an African savanna: relative influences of fire, herbivory, rainfall and density  
708 dependence. *Journal of Applied Ecology* **38**:268–280.

709 Schlesinger, W. H., and A. M. Pilmanis. 1998. Plant-soil interactions in deserts. *Biogeo-*  
710 *chemistry* **42**:169–187.

711 Schlesinger, W. H., J. A. Raikes, A. E. Hartley, and A. F. Cross. 1996. On the spatial  
712 pattern of soil nutrients in desert ecosystems: ecological archives E077-002. *Ecology*  
713 **77**:364–374.

714 Schlesinger, W. H., J. F. Reynolds, G. L. Cunningham, L. F. Huenneke, W. M. Jarrell,  
715 R. A. Virginia, and W. G. Whitford. 1990. Biological feedbacks in global desertification.  
716 *Science* **247**:1043–1048.

717 Sirami, C., and A. Monadjem. 2012. Changes in bird communities in Swaziland savannas  
718 between 1998 and 2008 owing to shrub encroachment. *Diversity and Distributions*  
719 **18**:390–400.

720 Skarpaas, O., and K. Shea. 2007. Dispersal patterns, dispersal mechanisms, and invasion  
721 wave speeds for invasive thistles. *The American Naturalist* **170**:421–430.

722 Sullivan, L. L., B. Li, T. E. Miller, M. G. Neubert, and A. K. Shaw. 2017. Density depen-  
723 dence in demography and dispersal generates fluctuating invasion speeds. *Proceedings*  
724 *of the National Academy of Sciences* **114**:5053–5058.

725 Taylor, C. M., and A. Hastings. 2005. Allee effects in biological invasions. *Ecology*  
726 *Letters* **8**:895–908.

727 Thompson, S. E., S. Assouline, L. Chen, A. Trahktenbrot, T. Svoray, and G. G. Katul.  
728 2014. Secondary dispersal driven by overland flow in drylands: Review and mechanistic  
729 model development. *Movement ecology* **2**:7.

730 Trollope, W., F. Hobson, J. Danckwerts, and J. Van Niekerk. 1989. Encroachment and  
731 control of undesirable plants. *Veld management in the Eastern Cape* pages 73–89.

- 732 Turnbull, L., J. Wainwright, and R. E. Brazier. 2010. Changes in hydrology and erosion  
733 over a transition from grassland to shrubland. *Hydrological Processes: An Interna-*  
734 *tional Journal* **24**:393–414.
- 735 Van Auken, O. 2009. Causes and consequences of woody plant encroachment into western  
736 North American grasslands. *Journal of environmental management* **90**:2931–2942.
- 737 Van Auken, O. W. 2000. Shrub invasions of North American semiarid grasslands. *Annual*  
738 *review of ecology and systematics* **31**:197–215.
- 739 Vasek, F. C. 1980. Creosote bush: Long-lived clones in the Mojave Desert. *American*  
740 *Journal of Botany* **67**:246–255.
- 741 Veit, R. R., and M. A. Lewis. 1996. Dispersal, population growth, and the Allee ef-  
742 fect: dynamics of the house finch invasion of eastern North America. *The American*  
743 *Naturalist* **148**:255–274.
- 744 Wang, M.-H., M. Kot, and M. G. Neubert. 2002. Integrodifference equations, Allee  
745 effects, and invasions. *Journal of mathematical biology* **44**:150–168.
- 746 Wells, P. V., and J. H. Hunziker. 1976. Origin of the creosote bush (*Larrea*) deserts of  
747 southwestern North America. *Annals of the Missouri Botanical Garden* pages 843–861.
- 748 Whitford, W., E. Depree, and P. Johnson. 1980. Foraging ecology of two chihuahuan  
749 desert ant species: *Novomessor cockerelli* and *Novomessor albigaster*. *Insectes Sociaux*  
750 **27**:148–156.
- 751 Whitford, W. G. 1978. Structure and seasonal activity of Chihuahua desert ant commu-  
752 nities. *Insectes Sociaux* **25**:79–88.
- 753 Wiernga, J. 1993. Representative roughness parameters for homogeneous terrain.  
754 *Boundary-Layer Meteorology* **63**:323–363.

- 755 Williams, J. L., T. E. Miller, and S. P. Ellner. 2012. Avoiding unintentional eviction  
756 from integral projection models. *Ecology* **93**:2008–2014.
- 757 Wood, S. 2017. *Generalized Additive Models: An Introduction with R*. 2 edition.  
758 Chapman and Hall/CRC.

## Appendix A: Dispersal kernel modeling

**WALD dispersal kernel** In order to create the dispersal kernel, we first take the wind speeds at measurement height  $z_m$  and correct them to find wind speed  $U$  for any height  $H$  by using the logarithmic wind profile <sup>5</sup>

$$U = \frac{1}{H} \int_{d+z_0}^H \frac{u^*}{K} \log \left( \frac{z-d}{z_0} \right) dz \quad (\text{A1})$$

given in Bullock et al. (2012) equation 6, with the notation slightly modified. Here,  $z$  is the height above the ground,  $K$  is the von Karman constant, and  $u^*$  is the friction velocity. The zero-plane displacement  $d$  and roughness length  $z_0$  are surface roughness parameters that, for a grass canopy height  $h$  above the ground, are approximated by  $d \approx 0.7h$  and  $z_0 \approx 0.1h$ . These estimates are from Raupach (1994) for a canopy area index  $\Lambda = 1$  in which the sum of grass canopy elements is equal to the unit area being measured. A 0.15 m grass height at our study site gives  $d = 0.105$  and  $z_0$ , which are suitable approximations for grassland (Wiernga, 1993). Calculations of  $u^*$  were done using equation A2 from Skarpaas and Shea (2007), in which

$$u^* = KU_m \left[ \log \left( \frac{z_m - d}{z_0} \right) \right]^{-1} \quad (\text{A2})$$

and  $U_m$  is the mean wind velocity at the measurement height  $z_m$ . Values for the turbulent flow parameter  $\sigma$  were then calculated using the estimate made by Skarpaas and Shea (2007) in their equation A4, where

$$\sigma = 2A_w^2 \sqrt{\frac{K(z-d)u^*}{C_0U}} \quad (\text{A3})$$

and  $C_0$  is the Kolmogorov constant.  $A_w$  is a constant that relates vertical turbulence to friction velocity and is approximately equal to 1.3 under the assumptions of above-

---

<sup>5</sup> *We need to describe and cite the wind data used here.*

canopy flow made by Skarpaas and Shea (2007), based off calculations from Hsieh and Katul (1997). In addition, the assumption that  $z = H$  was made in order to make the calculation of  $\sigma$  more feasible.<sup>6</sup>

The values from the previous three equations give us the necessary information to calculate  $\mu'$  and  $\lambda'$ , thus allowing us to create the WALD distribution  $p(r)$ . However, the base WALD model does not take into account variation in wind speeds or seed terminal velocities, which limits its applicability in systems where such variation is present. In order to account for this variation, we integrate the WALD model over distributions of these two variables using the same method as Skarpaas and Shea (2007). Additionally, the WALD model assumes seed release from a single point source, which is not realistic for creosote bush; because seeds are released across the entire height of the shrub rather than from a point source, we integrated  $p(r)$  across the uniform distribution from the grass canopy height to the shrub height. Thus, under the assumptions that the height at which a seed is located does not affect its probability of being released and that seeds are evenly distributed throughout the shrub, this gives the dispersal kernel  $K(r)$ , where

$$K(r) = \iiint p(F)p(U)p(z)p(r) dF dU dz \quad (\text{A4})$$

and  $p(F)$  and  $p(U)$  are the PDFs of the terminal velocity  $F$  and wind speed  $U$ , respectively, and  $p(z)$  is the uniform distribution from  $h$  to  $H$ .

**Dispersal data collection** The distribution  $p(F)$  in the integral above was constructed using experimentally determined seed terminal velocities. This was done by using laboratory-based seed release experiments with a high-speed camera and motion tracking software to determine position as a function of time. We then used the Levenberg-Marquardt algorithm to solve a quadratic-drag equation of motion for  $F$ . Before seeds were released, they were dried, dyed with yellow fluorescent powder, and then

---

<sup>6</sup> *Can you describe this assumption in biological terms?*



804 put against a black background to improve visibility and make tracking easier. While  
805 the powder added mass to the seeds, this added mass only yielded an approximately  
806 2.5% increase, likely having little effect on terminal velocities. Measurements were con-  
807 ducted for 48 seeds that were randomly chosen from a seed pool derived from different  
808 plants, and then an empirical PDF of terminal velocities was constructed using the data.  
809 Constructing  $p(U)$  involved creating an empirical PDF of hourly wind speeds using data  
810 from Sevilleta LTER meteorological station 49, the station closest to our transects. We  
811 used wind speed data collected hourly from 2015 to 2019 (Moore and Hall, 2022).

```
## Error in '[.data.frame'(aic_tables$surv_aic_out, , c("surv", "df", "dAIC"))':
undefined columns selected

## Error in align(surv_aic) <- "c|p{12cm}|c|c|": object 'surv_aic' not found

## Error in print(surv_aic, include.rownames = F, include.colnames = T, floating
= TRUE, : object 'surv_aic' not found
```

mean(size)	sd(size)	df	dAIC
~size + (1 transect)	~1	3.00	1024.88
~size + density + (1 transect)	~1	8.50	977.23
~size + density + size:density + (1 transect)	~1	10.47	975.17
~size + (1 transect)	~size	9.65	146.23
~size + density + (1 transect)	~size	16.24	19.45
~size + density + size:density + (1 transect)	~size	18.55	19.62
~size + (1 transect)	~size + density	10.40	115.52
~size + density + (1 transect)	~size + density	18.97	0.08
~size + density + size:density + (1 transect)	~size + density	21.33	0.00

Table B1: AIC model selection for mean and variance of future size

Pr(Flowering)	df	dAIC
~size + (1 transect)	5.78	0.63
~size + density + (1 transect)	6.80	2.32
~size + density + size:density + (1 transect)	7.24	0.00

Table B2: AIC model selection for flowering probability.

No. fruits	df	dAIC
~size + (1 transect)	14.25	71.99
~size + density + (1 transect)	5.52	0.00
~size + density + size:density + (1 transect)	6.23	0.37

Table B3: AIC model selection for fruit number.

Pr(Recruitment)	df	dAIC
$\sim(1 \text{transect})$	6.57	0.00
$\sim\text{density} + (1 \text{transect})$	7.39	0.93

Table B4: AIC model selection for recruitment probability.

mean(size)	sd(size)	df	dAIC
$\sim(1 \text{transect})$	$\sim 1$	2.00	2.90
$\sim\text{density} + (1 \text{transect})$	$\sim 1$	4.42	0.00
$\sim(1 \text{transect})$	$\sim\text{density}$	3.00	4.74
$\sim\text{density} + (1 \text{transect})$	$\sim\text{density}$	5.56	1.21

Table B5: AIC model selection for mean and variance of recruit size.